総　説
‖‖‖‖‖‖‖‖‖‖‖‖‖‖‖‖‖‖‖‖‖‖‖‖

中温域固体酸化物燃料電池用の電解質

Solid Electrolytes for Medium - Temperature Solid Oxide Fuel Cells

Hideaki INABA* and Hiroaki TAGAWA**

稲場　秀明* ・ 田川　博章**

Abstract

Fluorite oxide solid electrolytes with emphasis of doped ceria are reviewed in terms of electrical conductivity, diffusivity and transference number. The electrical conductivity and diffusion constant of various fluorite compounds are compared and those of ceria - based oxides are almost the highest among these fluorite oxides. The electrical conductivity of doped ceria is much dependent of the kind and the concentration of dopants. The reason for this behavior is qualitatively given as due to the defects associate between dopant cations and oxygen vacancies and the comparison between the theory and the experiment is presented. In order to decrease the activation energy in the electrical conductivity of doped ceria, it is suggested that the dopant cation with the critical radius, which is about 0. 111 and 0. 104 nm for di - valent and tri - valent cations, respectively, is desirable to choose. The effect of sample preparation on the electrical conductivity is described in terms of the character of raw materials, impurities and the sintering condition. The factors to determine the transference number and the methods to increase the transference number at low oxygen pressures are also described.

1. Introduction

The enviromental problems such as the increase in carbon dioxide in the atmosphere, acid rain and the destruction of forests and the contamination of seas and rivers are resulted from the large amount of energy consumption.

In order to solve the enviromental problems, it is necessary to maintain or decrease the total energy consumption. To develop the efficient systems of electric power generation is the urgent problem in order to save energy consumption. Solid oxide fuel cell is one of the important candidate of them.

Solid electrolytes have received increasing attention in recent years due to their excellent suitability as ionically conductive materials in high temperature systems, such as solid oxide fuel cells or oxygen sensors. Solid electrolytes with the fluorite structure have been extensively investigated and reviewed by Steele (1), Kilner and Steele (2), Sasaki (3) and Dell and Hooper (4). Among them, yttria - stabilized zirconia with the cubic fluorite structure has been the most extensively investigated and practically used.

The operating temperature for the solid oxide fuel cells using yttria - stabilized zirconia

横浜国立大学環境科学研究センター汚染拡散学（環境エネルギー科学）研究室
* Hideaki Inaba, Technical Research Laboratories, Kawasaki Steel Corporation, Guest Professor of the present Institute
** Hiroaki Tagawa, Department of Environmental Energy Science, Institute of Environmental Science and Technology, Yokohama National University, Yokohama, 240
（1994年10月30日受領）

usually taken as 1273K. It has been thought that 1273K is too high as the operating temperature of solid oxide fuel cells, because many interface reactions such as electrode/solid electrolyte, electrode /interconnector and interconnector/solid electrolyte would cause the decrease of the efficiency and the stability of the cells. The alternative solid electrolyte for yttria - stabilized zirconia has been awaited, which has the higher electric conductivity than that of yttria - stabilized zirconia with high ionic transference number and enables us to use at medium temperatures such as 1073K.

As the candidate for the alternative electrolyte, Bi_2O_3 and ceria - based electrolytes may be considered. The electrical conductivity including these oxides are shown in Fig. 1 according to Steele (1). It is seen from the figure that Bi_2O_3 and yttria - stabilized Bi_2O_3 are most electrically conductive. However, these oxides are easily reduced and evaporated under reductive atmospheres and they are not suitable for the electrolytes for the solid oxide fuel cells. Thus ceria - based electrolytes have collected much attention for the alternative of the yttria - stabilized zirconia as the electrolyte of the solid oxide fuel cell. As seen in Fig. 1, electrical conductivity of gadlinia - stabilized ceria is about one order of magnitude larger than that of yttria - stabilized zirconia and it is about $0.1\,Scm^{-1}$ at
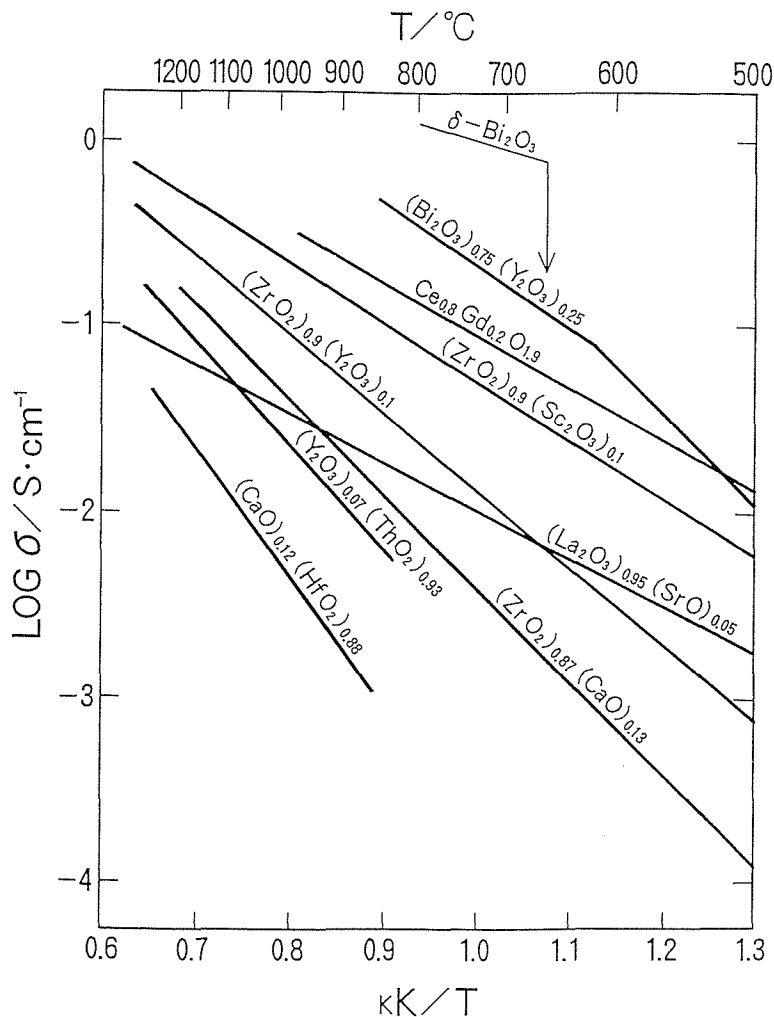

Fig. 1 Electrical conductivity of fluorite oxides (1)

1073K. It is noted, however, that ceria - based oxides are also reduced to give electronic conduction under reductive atmospheres. The magnitude of electrical conductivity and the stability under reductive atmospheres for ceria - based oxides are greatly dependent on the the kind and amount of doping elements, which have been critically reviewed here.

2. Experimental Aspects

2.1 Measurement of Electrical Conductivity

Historically measurements of the electrical conductivity have been made using dc four - prove method on sintered ceramic samples. This can lead to errors because of effects due to the grain boundaries and electrodes, which may mask the true behavior of the bulk. This uncertainty can be removed by the use of the complex plane impedance analysis (1, 2). In this method, the complex impedance Z of a specimen is

plotted as shown in Fig. 2, where the contributions due to the bulk, grain boundaries and electrodes are separated.

2.2 Measurement of Ionic Transference Number

The oxygen concentration cell, such as,

PO_2, Pt Electrode / (Solid Electrolyte) / Pt Electrode, $P'O_2$ (1)
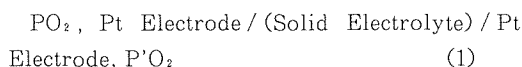
is usually used to obtain the ionic transference number of solid electrolytes as functions of temperature and oxygen partial pressure. The theoretical e.m.f. of the cell is given by

$$E_{theor} = (RT/4F) \ln (P'O_2 / PO_2), \quad (2)$$

where R is gas constant, T the absolute temperature and F Faraday's constant. The ionic transference number t_i is given by

$$t_i = E_{meas}/E_{theor.} \quad (3)$$

where E_{meas} is the observed open circuit e.m.f. for the cell. In the practical experiment, the one side of oxygen pressure (say $P O_2$) is fixed as air and the e.m.f. is obtained as a function of $P'O_2$.
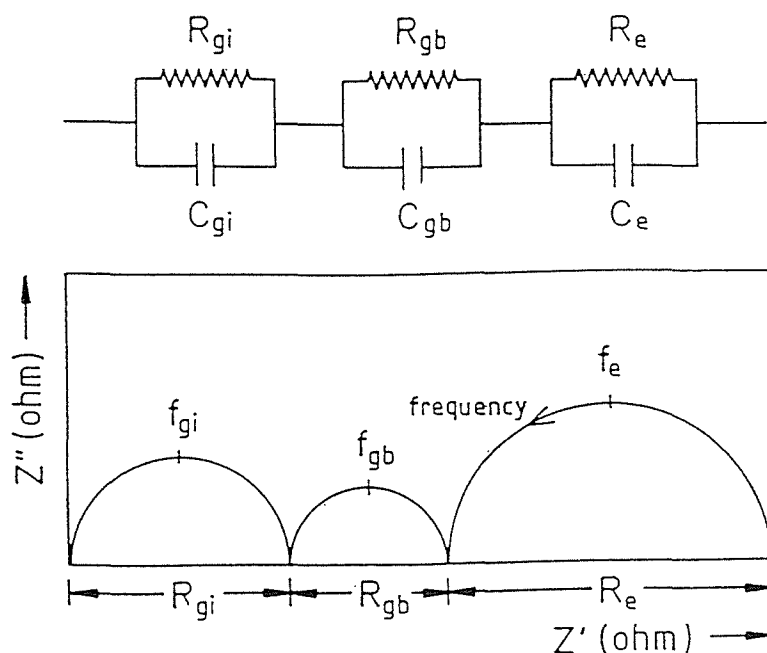

Fig. 2 Idealized equivalent circuit (a) and complex impedance diagram for a two phase ceramic electrolyte (b). R_{gi}, R_{gb} and R_e denote the electrical resistivity due to the bulk, grain boundary and electrode, respectively (1, 2).

3. Theoretical aspects

3.1 Temperature dependence of electrical conductivity

Oxides with high ionic conductivity have open structure, such as fluorite and pyrochlore. The ideal fluorite structure is shown in Fig. 3 (2).
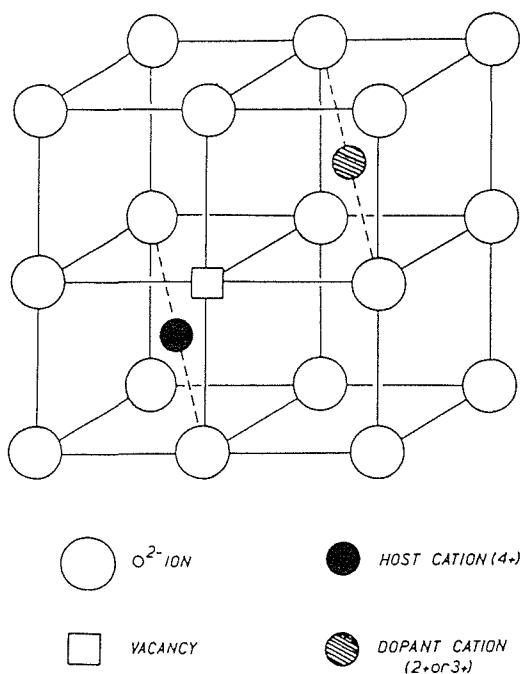

Fig. 3 A half unit cell of the fluorite structure showing the position of dopant cation - oxygen vacancy associate (2).

This structure is relatively open and it shows large tolerance for high levels of atomic disorder, which may be introduced either by doping, reduction or oxidation. Of the binary oxides, ThO_2, CeO_2, PrO_2, UO_2 and PuO_2 possess this structure in the pure state. ZrO_2 and HfO_2 are stabilized to the fluorite structure by doping with divalent or trivalent oxide. The addition of such dopants to these fluorite oxides gives rise to the creation of oxygen vacancies, which are responsible for the ionic conduction in these oxides.

The theory of electrical conduction has been described by Kilner and Steel (2) and Sasaki (3) and it is summarized here. The temperature dependence of the electrical conductivity σ of doped fluorite oxides has been empirically written as the following equation:

$$\sigma T = A \exp(-E_a/kT), \tag{4}$$

where A is a pre-exponential factor and E_a is the activation energy of electrical conduction. The ionic conductivity is given by the sum of the products of the concentration n_i and the mobility μ_i of charge carriers with charge q_i,

$$\sigma = \sum_i n_i q_i \mu_i \tag{5}$$

In the case of oxygen - ionic conductors, the conduction occurs via anion vacancies, so that

$$\sigma_v = C_v q_v \mu_v, \tag{6}$$

where the subscript v means anion vacancy and C_v is the number of anion vacancies per unit volume (cm^3). According to the Nernst - Einstein relation, the mobility is described with the corresponding diffusivity,

$$\mu = qB = qD/kT, \tag{7}$$

where B is absolute mobility. The diffusivity D is written as

$$D = a^2 v_0 \exp(\Delta S_m/k) \exp(-\Delta H_m/kT), \tag{8}$$

where a is jump distance of a vacancy, v_0 is an appropriate lattice vibration frequency and ΔS_m and ΔH_m are the activation entropy and activation enthalpy of diffusion, respectively. Since C_v is represented as:

$$C_v = [V_0] \{1 - [V_0]\} N_0, \tag{9}$$

where N_0 is the number of oxygen sites per unit volume, the following equations can be obtained using Eqs. (6), (7) and (8).

$$\sigma T = A' [V_0] \{1 - [V_0]\} \exp(-\Delta H_m/kT), \tag{10}$$

$$A' = (4e^2/k) a^2 v_0 N_0 \exp(\Delta S_m/k). \tag{11}$$

For small values of $[V_0]$, Eq. (10) can be approximated as

$$\sigma T = A' [V_0] \exp(-\Delta H_m/kT). \tag{12}$$

The temperature dependence of the electrical conductivity of doped fluorite oxides, however, cannot be expressed by a single exponential function shown in Eqs. (4), (10) or (12). The actual temperature dependence of the electrical conductivity in general is schematically shown in Fig. 4 according to Kilner and Walters (5), where three regions can be seen. In region I,
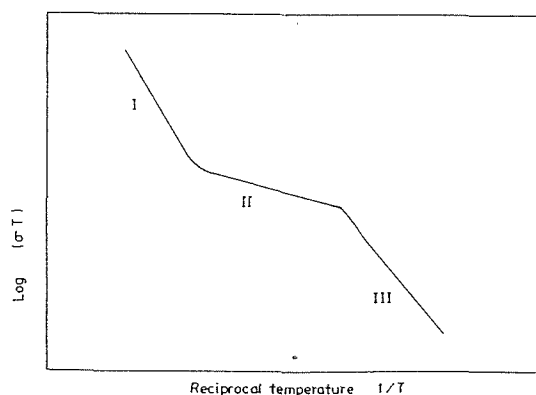
Fig. 4 A schematic representation of the conductivity behavior of an oxide ionic conductor (2).

which is appeared at high temperatures, the electrical conduction is determined by the intrinsic defects (Schottky or Frenkel) in the crystal.

In region II, electrical conduction is controlled by the population of charge carrying defects determined by an aliovalent dopant or impurity. In region III, the population of charge carrying defects is determined by the thermodynamic equilibrium between the free defects and the associated pairs. Since doped fluorite oxides have a large number of oxygen vacancies, they only have the regions II and III.

3.2 The effect of defect association

It would be reasonable to asume that the vacancies induced by doping of aliovalent cations are not free but are bound to dopant cations to form defect associates. This binding enthalpy is mainly due to the coulombic attraction of the defects caused by their effective charges in the lattice; however it also contains terms due to relaxation of the lattice around the defect, which depend on the effective charge, the size of the dopant and the cation polarizability. On the defect association, a detailed review was made by Kilner and Steele (2). They divided the situation of the defect associate into three possible cases.

The first case is that the dopant cation with the valence of 2 makes an associate with oxygen vacancy. Taking an example of Ca^{2+} in CeO_2, only one simple defect associate is possible;

$$\{ Ca''_M V_0^{\cdot\cdot} \}^x = Ca''_M + V_0^{\cdot\cdot} . \qquad (13)$$
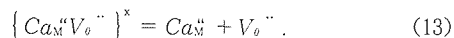
Applying the law of mass action to this equation gives

$$[Ca''_M][V_0^{\cdot\cdot}] / [\{ Ca''_M V_0^{\cdot\cdot} \}^x] = K_{A2} (T). \qquad (14)$$

Substituting the electrically neutral condition in the lattice: $[V_0^{\cdot\cdot}] = [Ca''_M]$, Eq. (14) is

$$[V_0^{\cdot\cdot}]^2 = [\{ Ca''_M V_0^{\cdot\cdot} \}^x] K_{A2} (T). \qquad (15)$$

For full association of defects,

$$[\{ Ca''_M V_0^{\cdot\cdot} \}^x] \gg [V_0^{\cdot\cdot}],$$

$$[\{ Ca''_M V_0^{\cdot\cdot} \}^x] = C_M, \qquad (16)$$

where C_M is the total dopant concentration expressed as a site fraction of the cation site.

This means that when no dissociation occurs all the dopant cations are bound to oxygen vacancies. The equilibrium constant K_{A2} can be expanded as

$$K_{A2} = (1/W) \exp(\Delta S_{A2}/k) \exp(-\Delta H_{A2}/kT), \qquad (17)$$

where W is the number of orientations of the associate and ΔS_{A2} and ΔH_{A2} are the entropy and enthalpy of association, respectively.

Substitution Eqs. (16) and (17) in Eq. (15) we obtain

$$[V_0^{\cdot\cdot}] = ([Ca''_M]/2W)^{1/2} \exp(\Delta S_{A2}/2k) \exp(-\Delta H_{A2}/2kT). \qquad (18)$$

Substitution of Eq. (18) into Eq. (12) gives

$$\sigma T = A' (C_M/2W)^{1/2} \exp[-(\Delta H_m + 1/2 \Delta H_{A2})/kT]. \qquad (19)$$

The second case is that the dopant cation cation with the valence of 3 makes an associate with oxygen vacancy; like Y^{3+} in CeO_2. In that case, the major defect is the associate of dopant and oxygen vacancy with one positive charge as

$$\{ Y'_M V_0^{\cdot\cdot} \}^{\cdot} = Y'_M + V_0^{\cdot\cdot} . \qquad (20)$$
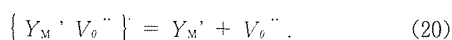
Then we obtain the following equation similarly as the first case as

$$\sigma T = (A'/W) \exp(\Delta S_{A1}/k) \exp[-(\Delta H_m + \Delta H_{A1})/kT]. \qquad (21)$$

The third case is that all the oxygen vacancies

to be free. In that case, we obtain

$$\sigma T = A' C_M \exp(-\Delta H_m/kT), \qquad (22)$$

where the electrical conductivity increases proportionally as the dopant concentration increases.

4. Experimental data on the electrical conductivity

4.1 General trends

The electrical conductivity of various types of fluorite oxides are shown in Fig.1 (1). The electrical conductivity is in the order of $\delta - Bi_2O_3 > CeO_2 > ZrO_2 > ThO_2 > HfO_2$ - related system. Among these, $\delta - Bi_2O_3$ has an oxygen deficient fluorite structure where 1/4 of the normal fluorite anion sites are vacant and shows the highest oxygen ion conductivity so far reported for the solid oxide electrolytes.

However, this oxide has little chemical stability; it is monoclinic structure at low temperatures and becomes cubic with ionic conduction
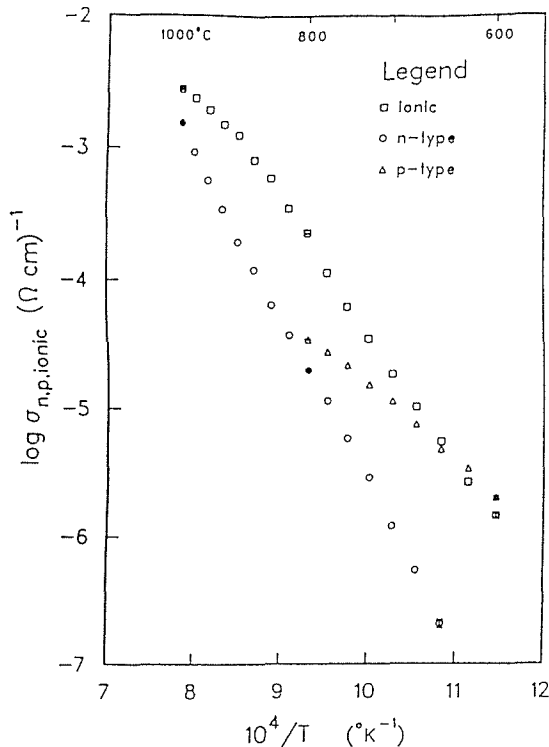
at high temperatures but easily reduced at low oxygen partial pressures (4). The pure CeO_{2-x} (more than 4N purity) is a mixed conductor with almost the same partial conductivities of oxygen ion, electron and hole according to Panhans and Blumenthal (6). The partial conductivities of $3NCeO_{2-x}$ at 1 atm oxygen pressure are shown in Fig.5 (6), where the ionic conductivity is significantly increased by the impurity atoms such as Na_2O, CaO and SrO.

The additive effect of alkaline earth oxides as dopants in ceria such as CaO, SrO, MgO and BaO was studied by Arai et al. (7, 8) and the electrical conductivity of these doped oxides is shown in Fig.6. As seen in Fig.6, the addition of CaO and SrO enhances electrical conductivity,
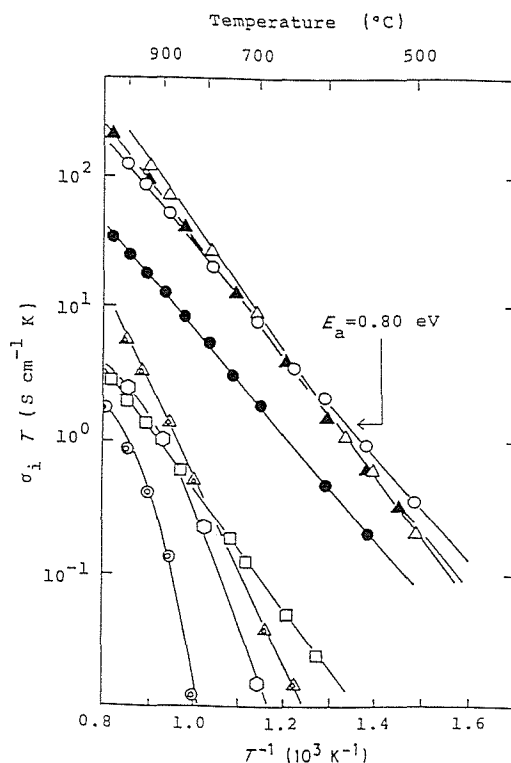

Fig. 5 Partial conductivities of ionic, n - type and p - type at 1 atm oxygen pressure from fit for 3N CeO_{2-x} (6).

Fig. 6 Arrhenius plots of ionic conductivity of ceria based oxides doped with alkaline - earth oxides according to Yashiro et al. (7). $\triangle$: $(CeO_2)_{0.9}$ $(CaO)_{0.1}$, $\blacktriangle$: $(CeO_2)_{0.7}$ $(CaO)_{0.3}$, $\bigcirc$: $(CeO_2)_{0.9}$ $(SrO)_{0.1}$, $\bullet$:$(CeO_2)_{0.7}$ $(SrO)_{0.3}$, $\square$: $(CeO_2)_{0.9}$ $(BaO)_{0.1}$, $\bigcirc$: $(CeO_2)_{0.9}$ $(MgO)_{0.1}$, $\triangle$: $(ZrO_2)_{0.85}$ $(CaO)_{0.15}$, $\circledcirc$: CeO_2

of ceria and makes the activation energy lower.

The addition of BaO and MgO, however, does not increase the electrical conductivity very much as compared with CaO and SrO. The additive effect of various rare earth oxides as dopants in ceria on the electrical conductivity has been studied by many investigators (9 - 16).

Electrical conductivity of ceria doped with 10 mol% Sm_2O_3, Gd_2O_3, Pr_2O_3, Y_2O_3, Tb_2O_3 and Er_2O_3 reported by Yashiro et al. (9) and Balags and Glass (10) are shown in Fig.7 and 8, respectively, where $Ce_{0.8} Sm_{0.2} O_{1.9}$ is seen to be the highest electrical conductivity among ceria - based oxides.

Electrical conductivities of ceria doped with 10 mol% rare earth (M_2O_3) and alkaline earth (MO) oxides at 1073K obtained from the data by
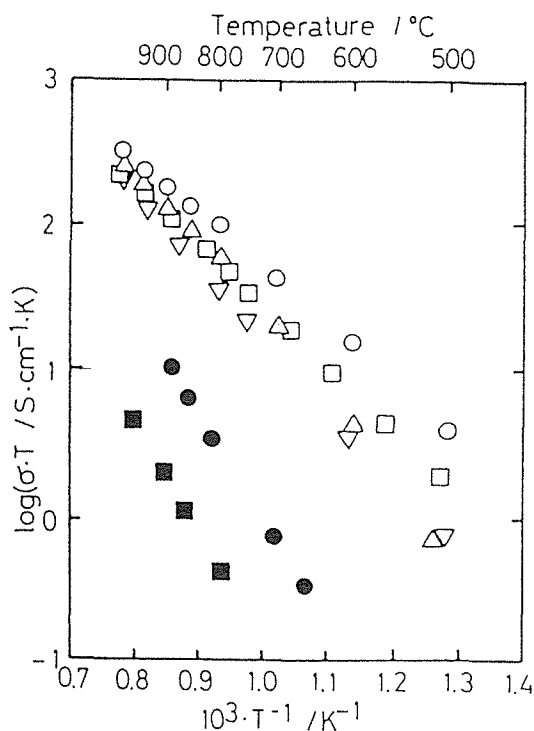

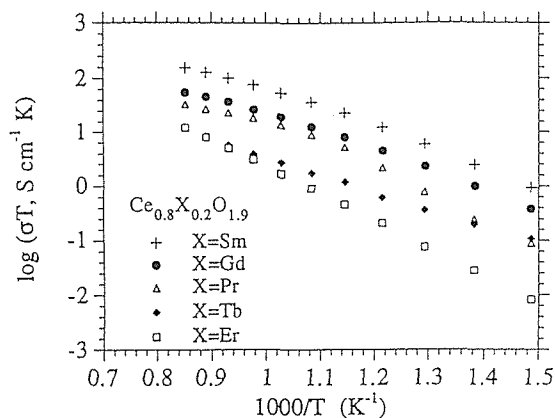**Fig. 8** Ionic conductivity of ceria doped with 10 mol% Sm_2O_3, Gd_2O_3, Pr_2O_3, Tb_2O_3 or Eb_2O_3 according to Balazs and Glass (10).

Fig. 7 Arrhenius plots of ionic conductivity of ceria based oxides doped with rare - earth oxides according to Yashiro et al. (9). O: $(CeO_2)_{0.8} (SmO_{1.5})_{0.2}$, △: $(CeO_2)_{0.8} (GdO_{1.5})_{0.2}$, ▽: $(CeO_2)_{0.8} (YO_{1.5})_{0.2}$, □: $(CeO_2)_{0.8} (CaO)_{0.2}$, ■: CeO_2, ●: $(ZrO_2)_{0.85} (YO_{1.5})_{0.15}$

Yashiro et al. (9) and Eguchi et al.(11) are plotted against the radius of dopant ion in Fig.9. The doping of Sm^{3+} ion among rare earth oxides and Ca^{2+} ion among alkaline earth oxides with an ionic radius of about 0. 11 nm gives the maximum electrical conductivity. The maximum electrical conductivity at this radius of dopant ion is the similar ionic radius as the host ion resulting in the minimum association enthalpy between dopant ion and oxygen vacancy, which will be discussed in the next section. The electrical conductivities doped with MgO and BaO are exceptionally low as seen in Fig.9 (7), which may be ascribed to the insufficient solubility of these oxides in ceria , as the lattice parameter of ceria - alkaline earth oxides is shown in Fig.10 (7).

The lattice parameter of ceria doped with rare earth oxides as a function of dopant concentration was measured by Bevan and Summerville (17) and it is shown in Fig.11, where higher solubility of rare earth oxides can be seen. It is also seen in Fig.11 that the lattice parameter of these doped ceria is much dependent on the kind of dopants. The linear relationship between the lattice parameter and the radius of dopant cations has been observed by Yashiro et al. (9), which is shown in Fig.12.
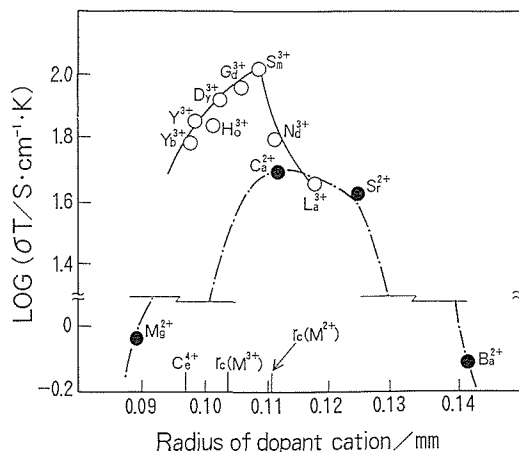
Fig. 9 Ionic conductivity of doped ceria at 1073K against the radius of dopant cation. r_c shown in the horizontal axis is the critical radius of the di - valent or tri - valent cation (7, 9, 11, 21).
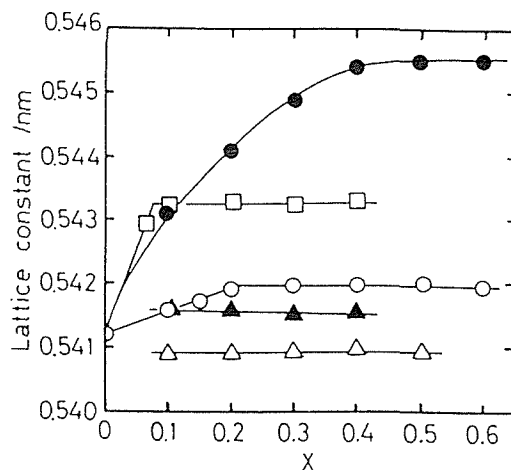

Fig. 10 Lattice constants of ceria based oxides, : $(CeO_2)_{1-x}(MO_y)_x$, as a function of dopant concentration, x, where y=1 except for y=1.5 in M=Sm according to Yashiro et al. (7). M: ●; Sm, △; Mg, ○; Ca, □; Sr, ▲; Ba

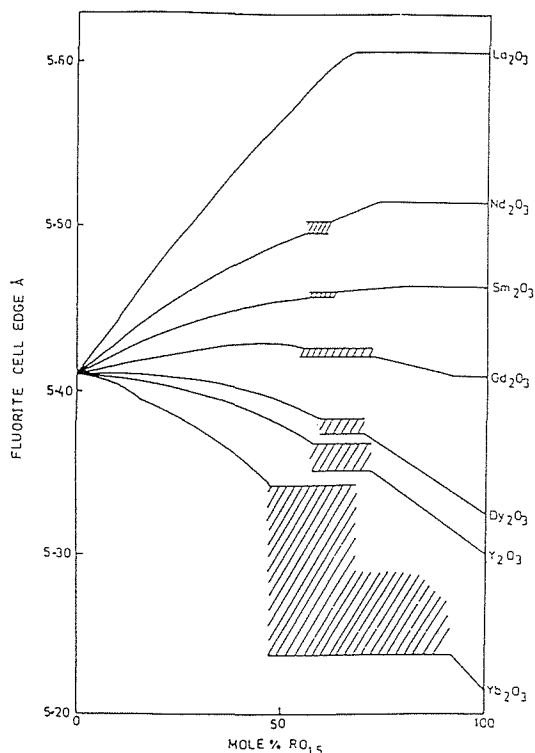Fig. 11 The variation of lattice parameter with dopant concentration for the fluorite oxides $Ce_{1-x}R_xO_{2-y}$ (17).
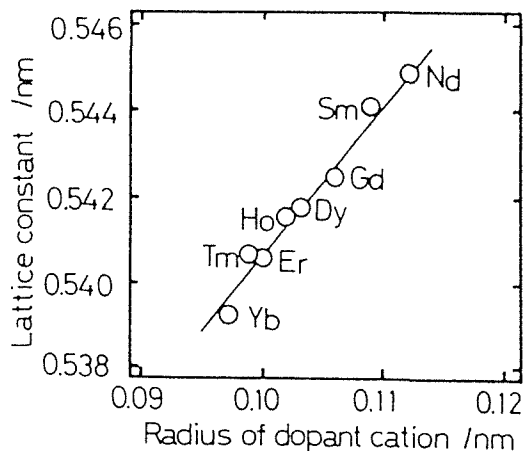

Fig. 12 Lattice constant of doped ceria $Ce_{0.8}R_{0.2}O_{2-y}$ against the ionic radius of dopant cation (9).

4.2 The dependence of dopant concentration on the electrical conductivity

The electrical conductivities of ceria doped with alkaline - earth oxides, Sm_2O_3 and Y_2O_3 were measured by Yashiro et al. (7, 14) and Wang et al. (15) and is shown as a function of dopant concentration in Fig.13, 14 and 15, respectively.

The maximum conductivity is obtained at 10 mol% for alkaline - earth oxides (MO) and Sm_2O_3 and 4% for Y_2O_3. The activation energy for various rare earth oxides as a function of dopant concentration was studied by Faber et al. (16) and it is shown in Fig.16. It shows a minimum value at a certain concentration depending on the dopant cations. The behaviors shown in Fig.13 - 16 suggest that there are some interactions between dopant ions and oxygen vacancies and the concentration of oxygen vacancy shown in Eq. (1?) is a complex function of dopant concentration depending on the dopant.

It is also noted here that the maximum of the electrical conductivity and the minimum of the activation energy are not always associated with the the same dopant concentration as seen in Fig.15, because the pre - exponential factor is also a function of the dopant concentration and the dopant concentration corresponding to the maximum of the conductivity depends on temperature.
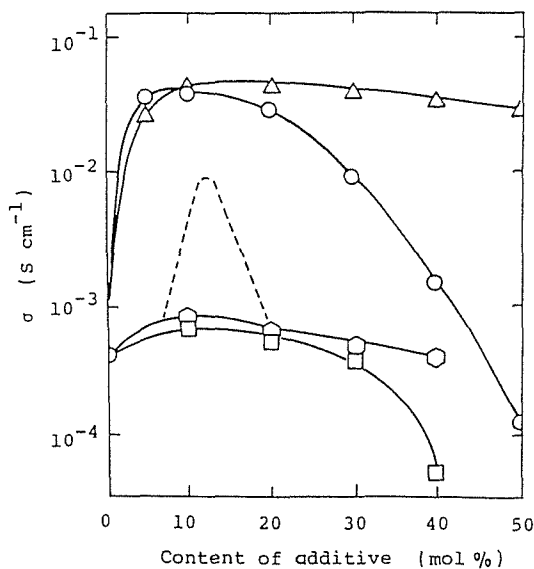

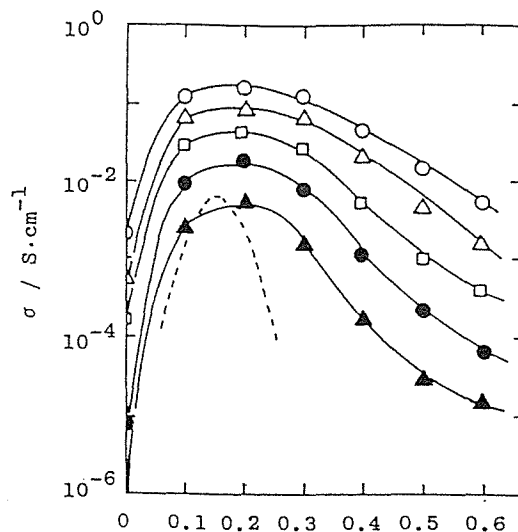
Fig. 14 Concentration dependence of conductivities for $(CeO_2)_{1-x}$ $(SmO_{1.5})_x$ (14). $\bigcirc$; 900℃, $\triangle$: 800℃, $\square$: 700℃, $\bullet$: 600℃, $\blacktriangle$: 500℃, $- - -$: $(ZrO_2)_{1-x}$ $(CaO)_x$ at 800℃.

Fig. 13 Conductivities of ceria - alkaline earth oxides systems at 1073K as a function of dopant (7). $\triangle \cdot (CeO_2)_{1-x}$ $(SrO)_x$, $\bigcirc$ $(CeO_2)_{1-x}$ $(CaO)_x$, $\square$ $(CeO_2)_{1-x}$ $(BaO)_x$, $(CeO_2)_{1-x}$ $(MgO)_x$, $- - -$ $(ZrO_2)_{1-x}$ $(CaO)_x$.
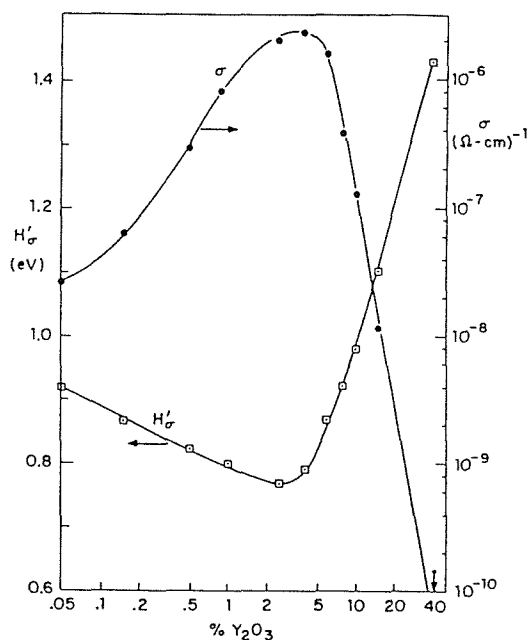

Fig. 15 Variation of the low temperature activation enthalpy, H_σ' with concentration, the latter plotted on a logarithmic scale. Also shown is the conductivity at 182℃ as a function of concentration (15).
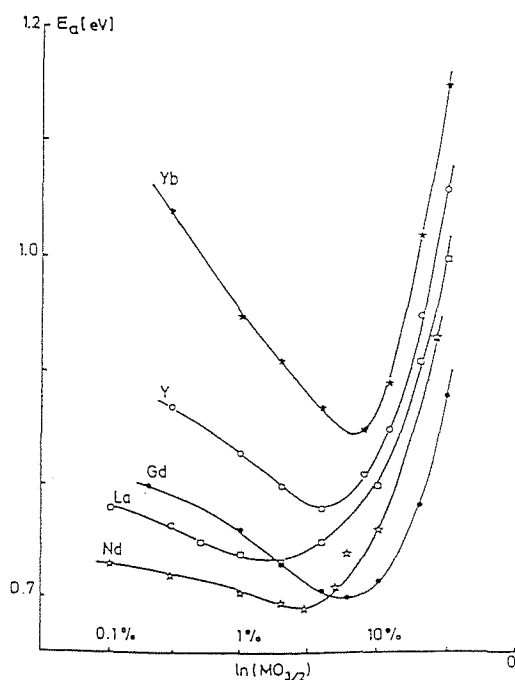
Fig. 16 Activation energy against dopant concentration for various doped cerias (16).

5. Interpretation of the electrical conductivity

5.1 The relation between association enthalpy of defect associate and ionic radius of dopants

As has been shown in the previous section, the maximum electrical conductivity was obtained at the radius of dopant ion similar to the ionic radius of the host ion. This fact shows that there is an optimum ionic radius of the dopant ion, which gives the minimum association enthalpy between dopant ion and oxygen vacancy. Kilner and Steele (2) emphasized the importance of the defect pairs between oxygen vacancies and aliovalent cations as shown in Eq. (20). The total activation energy is thus given by the following expression:

$$\Delta Ea = \Delta H_m + \Delta H_A, \qquad (23)$$

where ΔH_A is the association enthalpy of the complex defect such as $\left\{ Y_M \,\raisebox{0.3ex}{,}\, V_0^{\cdot\cdot} \right\}$ The enthalpy for migration ΔH_m can be estimated

as 0.5 eV according to Faber et al. (16) or 0.61 eV according to Wang et al. (15) and then ΔH_A is calculated from the experimental value of ΔE_a.

The theoretical calculation of the association enthalpy on ceria doped with some rare earth oxides was conducted by Butler et al. (18) assuming the fully ionic model, Born - Mayer potential for short range interionic forces and the shell model for the ionic polarization. The results are shown in Fig.17 together with the experimental results by Gerhardt - Anderson and Nowick (12). Figure 17 shows that the theoretical calculation predicts quantitatively the association enthalpies of the associate. Kilner (19) has pointed out referring the similar relation in doped MgO system that the dependence of association enthalpy on dopant size is much smaller for ions lager than the host than for those smaller than the host cation size. The similar relation between activation energy and dopant radius on rare earth - doped zirconia was given by Kilner and Brook (20) and it is shown in Fig.18. It would be necessary, however, to make a small but important modification about this theoretical analysis as pointed out by Kim (21). He derived the empirical equations for the lattice parameters of fluorite - related oxides doped with various valent cations considering the charge effect as well as the difference of ionic radius between the host and dopant ions. For the radius of cations the 8 - coordinated values compiled by Shannon and Prewitt (22) were chosen. He proposed the critical radius, r_c, in order to better understand the relation between association enthalpy and dopant radius, which corresponds to the ionic radius of the dopant whose substitution for the host cation causes neither expansion nor contraction in the fluorite lattice. The critical radii, r_c, for di - valent and tri - valent cations as dopants in ceria are calculated as 0.1106 and 0.1038 nm, respectively, which are much closer to the radii of dopants corresponding to the maximum electrical conductivity as shown in Fig.9 as compared with the radius of host ion. In Fig.19, the critical

radius for several different valencies is plotted as a function of host cation radius. He also calculated the deviation of the lattice parameter from the hypothetical pure zirconia in the system of ZrO_2 - ThO_2 - Y_2O_3 (21). The activation energy of the electrical conduction can thus be correlated with the deviation of the lattice parameter from the hypothetical pure zirconia as shown in Fig.20.
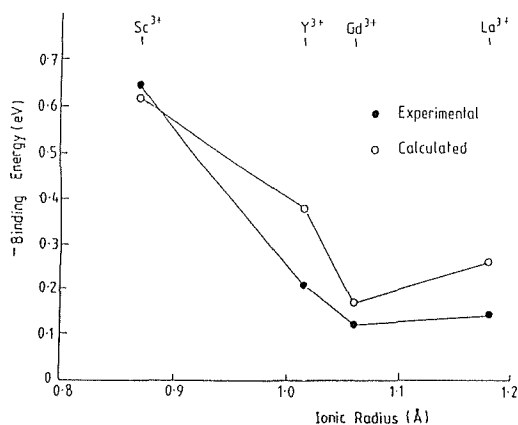

Fig. 19 Critical dopant radius, r_c, in the fluorite lattice as a function of host cation radius for dopants of several different valencies (21).

Fig. 17 Calculated and observed association enthalpy of the defect associate of doped ceria against ionic radius of dopant cation (18).

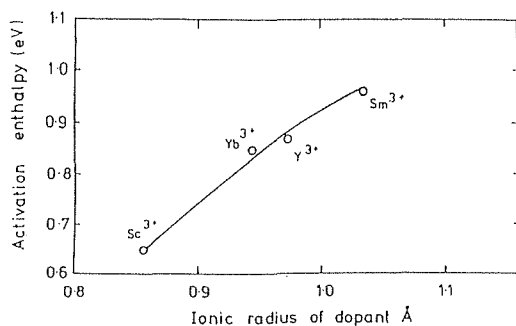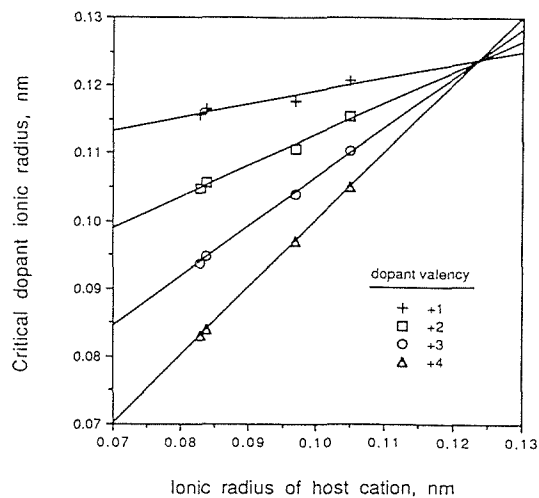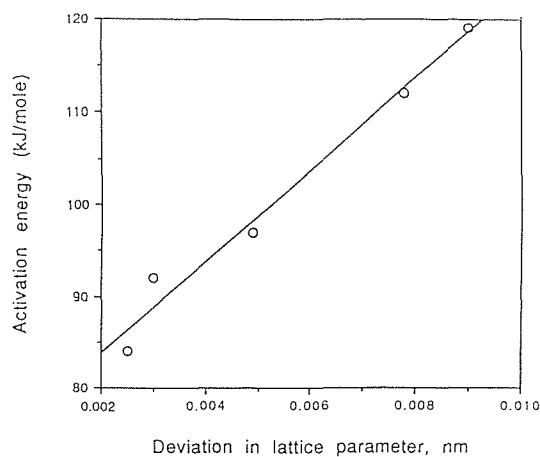**Fig. 20** Activation energy for conduction in the system ZrO_2 - ThO_2 - Y_2O_3 against the deviation in the lattice parameter from the hypothetical pure ZrO_2 (21).

Fig. 18 Activation energy for conduction in doped zirconia as a function of ionic radius of dopant cation (20).

Steele (1) further proposed that because the association enthalpy is dependent on the relative radii of host and dopant, plots of lattice parameter versus concentration should yield relevant qualitative information about the expected strain component, and derived values for ThO_2, $BiO_{1.5}$, CeO_2 and ZrO_2 host lattices

together with the rare earth elements are shown in Fig.21. It can be drawn from Fig. 21 that Th^{4+} is, in general, too large a host cation; most dopants are smaller and high strain components are predicted and Zr^{4+} is, in general, too small a host cation as most dopant cations have larger radius.
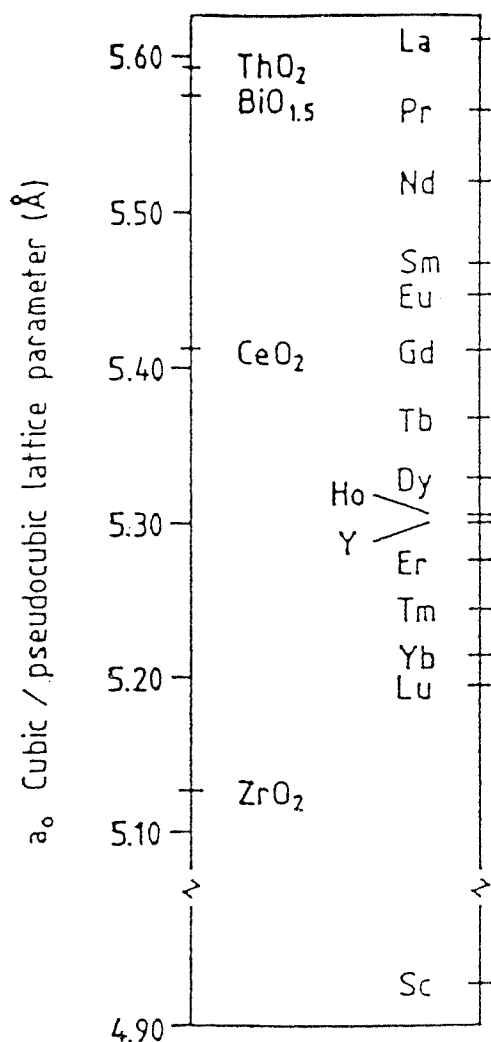

Fig. 21 Lattice parameter maps of the various fluorite oxides (1).

5. 2 Activation energy and pre - exponential term

As has been described in the previous section , the activation energy is the sum of the mobility enthalpy and association enthalpy. The mobility enthalpy of doped ceria was taken as 0. 5 eV by Faber et al. (16) considering the results of NMR study (23) and 0. 61 eV by Wang et al. (15) taking into account the activation energy of pure ceria and doped ceria. Since the mobility enthalpy is considered to be independent of dopant, the variation of the activation energy with dopants can be acribed to the asociation enthalpy. The activation energy of calcia - doped ceria is obtained as 0. 83 - 0. 89 eV over the concentration range up to 80% CaO according to Arai et al. (8); almost no compositional dependence is obtained as expected from Eq. (13), where the defect associate has no effective charge and no further interactions between defects are expected.

The concentration dependence of association enthalpy in a low concentration range of Y$_2$O$_3$ was analyzed by Wang et al. (15). The unique feature of rare earth - doped ceria is that the defect association involves incomplete compensation; i.e. the $\{ Y_M{}' \; V_0{}^{..} \}$ pair retains a residual charge, as do the remaining isolated $Y_M{}'$ defects. They derived the following equations assuming the energetically fovorable electrostatic interaction between the defects and the surrounding charges:

$$H_A = H_A{}^0 - \Delta E_{int}, \qquad (24)$$

$$\Delta E_{int} = 0. 42 \, c_0{}^{1/3}/\beta, \qquad (25)$$

where $H_A{}^0$ is the association enthalpy at infinite dilution, ΔE_{int} is the mean interaction energy with the surrounding charges involved in the process of association, c_0 is the dopant concentration and β is a dimensionless parameter for averaging the electric field. The fitting of the theoretical equation to the experimental results is shown in Fig. 22, where H_A decreases and the electrical conductivity increases with the 1/3 power of the yttria concentration over the dilute range as shown in Eq. (25).

Adler and Smith (24) demonstrated the importance of long-range forces on the oxygen transport in yttria - doped ceria using the Monte Carlo simulation based on the point defect model with a Debye - Hückel modification.

The simulated ionic conductivity of yttria - doped ceria is shown in Fig. 23, where "extent parameter" λ : the range of Coulombic forces is given as infinite, otherwise it does not explain the experimental results. These theoretical

(16) and are shown in Figs. 24 and 25, respectively, where the numbers marked in the figures denote the order of the concentration. As the concentration of the dopants increases, the
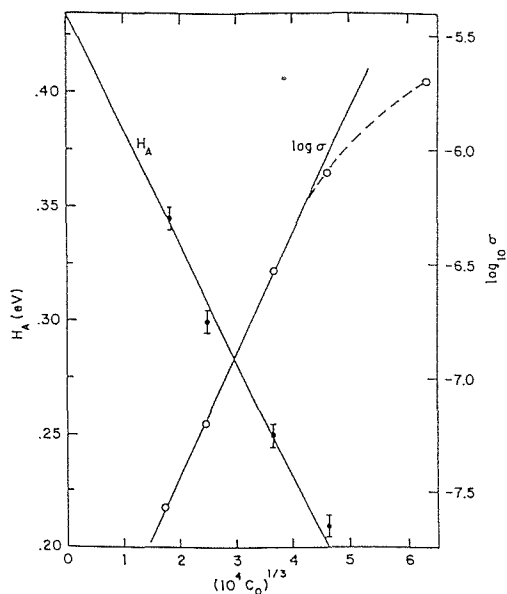

Fig. 22 Variation of activation energy and log σ (at 182 ℃) with 1/3 power of the yttria concentration over the yttria concentration over the dilute range (15).

Fig. 23 Simulated ionic conductivity of yttria-doped ceria for the case of Coulombic forces between particles (the extent parameter is taken as infinity). The dashed lines are the predictions of an ideal point - defect model. The solid lines are the predictions based on a point defect model which includes a Debye - Hückel correction. Dopant concentrations are quoted in mol% Y_2O_3 in CeO_2 (24).

analyses can only be applied to a dilute range of dopant concentration; they collapse around the concentration of the maximum electrical conductivity.

As already described, the maximum of the electrical conductivity and the minimum of the activation energy are not necessarily associated with the same dopant concentration, because the pre - exponential factor is also a function of concentration. The electrical conductivity and the pre - exponential term of yttria - and gadlinia - doped ceria are plotted as a function of the activation energy using the data by Faber et al.
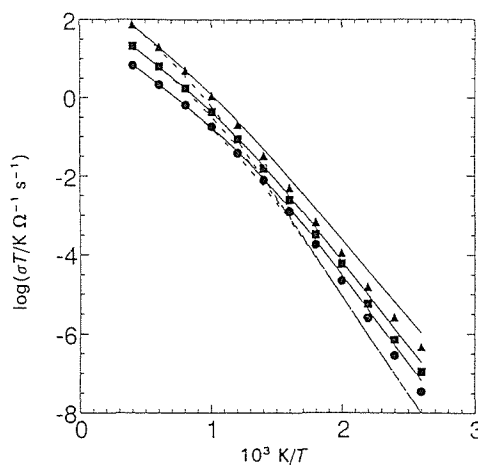
activation energy decreases significantly while the pre - exponential term keeps almost constant. The pre - exponential term begins to increase significantly after the activation energy becomes minimum. The maximum electrical conductivity is obtained at a higher concentration than that at the minimum activation energy. It is noted that the concentration which gives the maximum electrical conductivity is quite different between yttria - and gadlinia-doped ceria; 4% for yttria - and 10% for gadlinia - doped ceria. The pre - exponential term begins to decrease at higher concentrations.
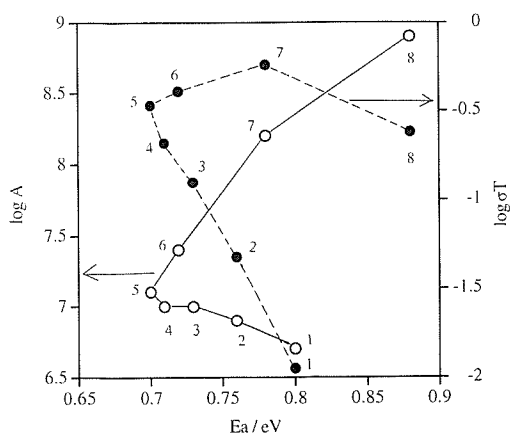
216

Fig. 24 The pre-exponential factor (log A) and the electrical conductivity (log σ T at 1073K) of yttria-doped ceria as a function of the activation energy (16). The numbers marked in the figure show the concentration of yttria as follows; 1 : 0.05%, 2 : 0.15%, 3 : 0.5%, 4 : 1%, 5 : 2%, 6 : 4%, 7 : 6%, 8 : 10%, 9 : 15%.
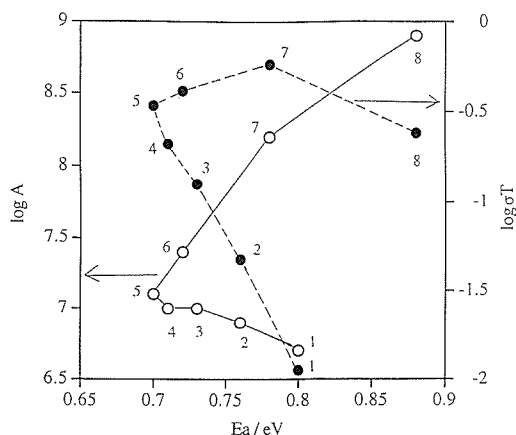
Fig. 25 The pre-exponential factor (log A) and the electrical conductivity (log σ T at 1073K) of gadlinia-doped ceria as a function of the activation energy (16). The numbers marked in the figure show the concentration of gadlinia as follows; 1 : 0.1%, 2 : 0.5%, 3 : 1%, 4 : 2%, 5 : 3%, 6 : 5%, 7 : 10%, 8 : 15%.

The concentration dependence of pre-exponential factor in doped fluorite oxides has not been well understood yet, but this dependence may come from the ΔS_{A1} term in Eq. (21), because other terms are considered to be independent on the concentration. The decrease in the pre-exponential term at the higher dopant concentrations may be due to the partial ordering of the defects. The partially ordered structures were detected by Allpress and Rossell (25) by means of electron diffraction using annealed samples of calcia-stabilized zirconia and hafnia, which showed lower electrical conductivity as compared with the sample of no annealing.

6. Diffusivity

The diffusion constants of fluorite-related compounds obtained from the various literatures (26-39) are compiled and shown in Fig. 26, where the diffusion constants in the

anion sublattice (O, F, or Cl) are shown. The diffusion constants in the anion sublattice are several orders of magnitude lager than those of cation sublattice, which were compiled by Oishi et al. (26, 27). It is noted that the activation energies of stoichiometric compounds such as UO_2, ThO_2, PuO_2, CaF_2 $SrCl_2$, and BaF_2 are much higher than those of nonstoichiometric compounds and doped solid solutions. This phenomenon may be understood using the following equation:

$$E_a = \Delta H_m + \Delta H_f, \qquad (26)$$

where ΔH_f is the enthalpy of vacancy formation. In the case of stoichiometric compounds, ΔH_f has a large value because almost all the anions in the sublattice are occupied; while in the case of nonstoichiometric compounds or doped solid solutions, anion vacancies are already present in some forms and there is no need to create anion vacancies. The term represented by ΔH_f (ΔH_A in this case) may be
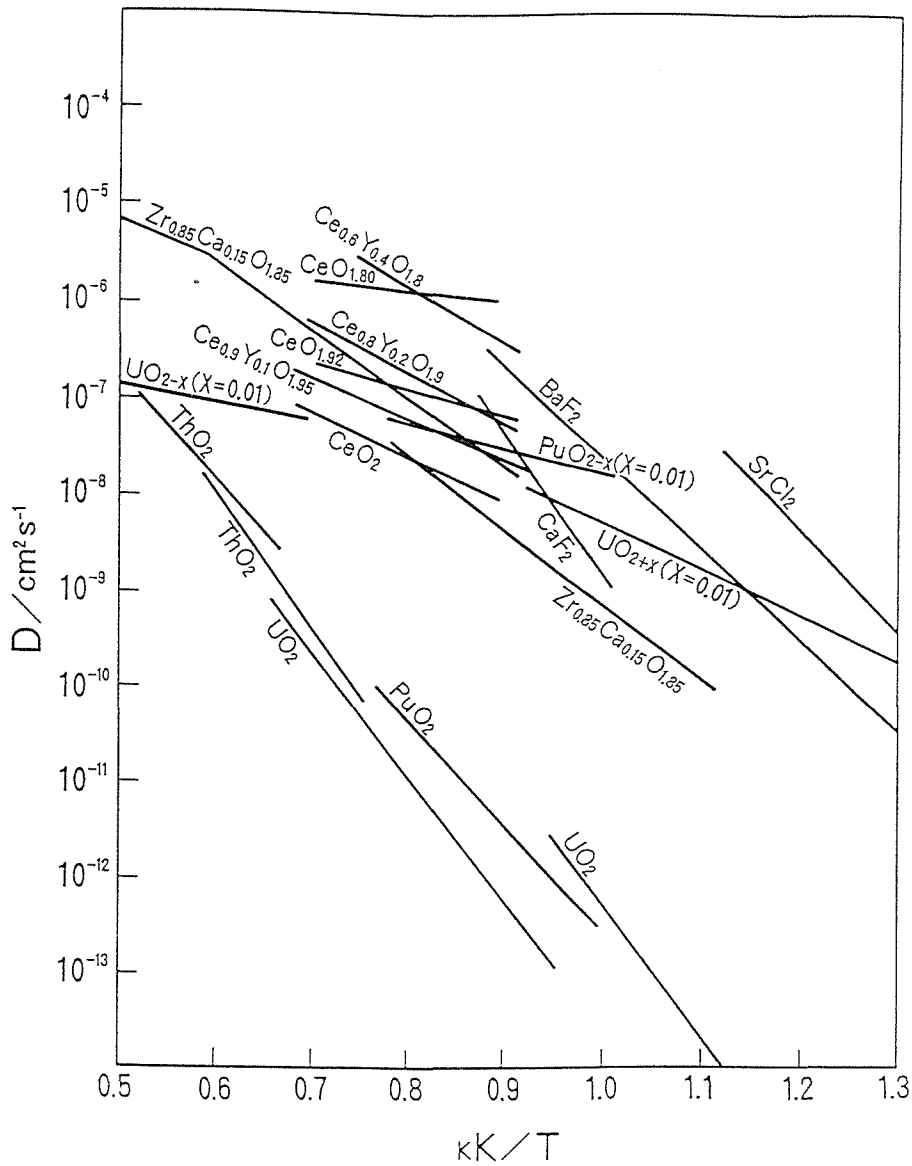
Fig. 26 Diffusion constants of anion sublattice in various fluorite compounds.
⑦ $Zr_{0.85}Ca_{0.15}O_{1.85}$ (26), ⑧ CaF_2 (28), ⑨ BaF_2 (29), ⑩ $SrCl_2$ (29), ⑪ $Ce_{0.6}Y_{0.4}O_{1.8}$ (30), ⑫ $Ce_{0.8}Y_{0.2}O_{1.9}$ (30), ⑬ $Ce_{0.9}Y_{0.1}O_{1.95}$ (30), ⑭ CeO_2 (30), ⑮ $Zr_{0.85}Ca_{0.15}O_{1.85}$ (31), ⑯ UO_2 (32), ⑰ PuO_2 (33), ⑱ UO_2 (34), ⑲ ThO_2 (35), ⑳ ThO_2 (36), ㉑ UO_{2-x} (x=0.01) (37), ㉒ PuO_{2-x} (x=0.01) (38), ㉓ UO_{2+x} (x=0.01) (39), ㉔ $CeO_{1.8}$ (30), ㉕ $CeO_{1.92}$ (30).

assigned as some interaction term between defects, which is much smaller than that of stoichiometric compounds.

In order to compare these diffusion constants with those of doped fluorite oxides shown in Fig. 1, the electrical conductivity is converted into the diffusion constant using the Nernst-Einstein relation as the following equation:

$$D = \sigma kT t_i / (4 C_v e^2) = \sigma kT t_i a_0^3 / (16 \delta e^2), \quad (27)$$

where a_0 and δ is the lattice parameter and the molar vacant concentration in the form of $MO_{2-\delta}$, respectively, the quadratic term on oxygen vacancy in Eq. (9) is neglected and the correlation factor of the diffusion is assumed to be unity. The lattice parameters of various doped fluorite oxides are obtained from the empirical equations given by Kim (21). The converted diffusion constants from the electrical conductivities are shown in Fig. 27, where the diffusion constants of various fluorite compounds shown in Fig. 26 are also shown for comparison. It is seen from Fig. 27 that δ - Bi_2O_3, gadlinia - doped ceria and yttria - doped zirconia give the highest diffusion constants among these fluorite compounds, which are known as solid electrolytes. The activation energies of the diffusion for these solid electrolytes lie somewhere between those of stoichiometric compounds and nonstoichiometric compounds, since the behaviors of the activation energy of doped fluorite oxides are mainly determined by those of the defect associates as described in the previous section.

The plot of the diffusion constants of various fluorite compounds against the normalized temperature: the temperature divided by the melting point, was first conducted by Matzke (40) and then Oishi et al. (26, 27). The diffusion constants of various fluorite compounds shown in Fig. 27 are plotted against the normalized temperature as shown in Fig. 28, where the unknown melting points such as gadlinia-doped ceria and yttria-doped ceria are assumed to be the same as the pure oxides such as ceria.

In Fig. 28, the diffusion constant is represented as:

$$D = D_0 \exp \left(- \frac{E_a / T_m}{kT / T_m} \right), \quad (28)$$

where D_0 is frequency factor and T_m is the melting point. It was shown by Oishi et al. (26, 27) that the diffusion constant against the normalized temperature plot of cation sublattice was tend to be converged in a single line, but that for anion sublattice was rather scattered as being characteristic as the liquid - like behavior even at low temperatures. It should also be noted that the diffusion constant of anion sublattice is very sensitive to the nonstoichiometry and impurities of sample such as a large difference in that between UO_2 and UO_{2-x} ($x = 0.01$) as seen in Fig. 27 and these effects also contribute to the scatter in Fig. 28.

Nevertheless, the diffusion constants at the melting point ($T/T_m = 1$) tend to be around the value 10^{-4} cm²s⁻¹ in Fig. 28, which shows the diffusion constant of a liquid. It is noted that δ - Bi_2O_3 (① in Fig. 28) lies just close to the melting point, which is in quite different position in Fig. 27.

7. Transference number

The total electrical conductivity σ_t of solid is the sum of the contributions due to ion, electron and hole as follows;

$$\sigma_t = \sigma_{ion} + \sigma_e + \sigma_h, \quad (29)$$

where ion, e and h mean ion, electron and hole, respectively. These partial conductivities are expressed according to Patterson(41) by

$$\sigma_{ion} = \sigma^0_{ion} \exp \left(- Q_{ion} / kT \right) \quad (30)$$

$$\sigma_h = \sigma^0_h P_{x_2}^{1/n} \exp \left(- Q_h / kT \right) \quad (31)$$

$$\sigma_e = \sigma^0_e P_{x_2}^{-1/n} \exp \left(- Q_e / kT \right), \quad (32)$$

where X_2 is gas (in the case of oxides, O_2), P is the partial pressure of gas, σ^0 and Q are pre-exponential factor and activation energy, respectively, and n is the factor determined by the predominant defect structure. The conduction domains are determined by using Eqs. (30 - 32) and they are schematically shown in Fig. 29. The electrolyte domain is determined by measuring the transference number of ion, t_i,
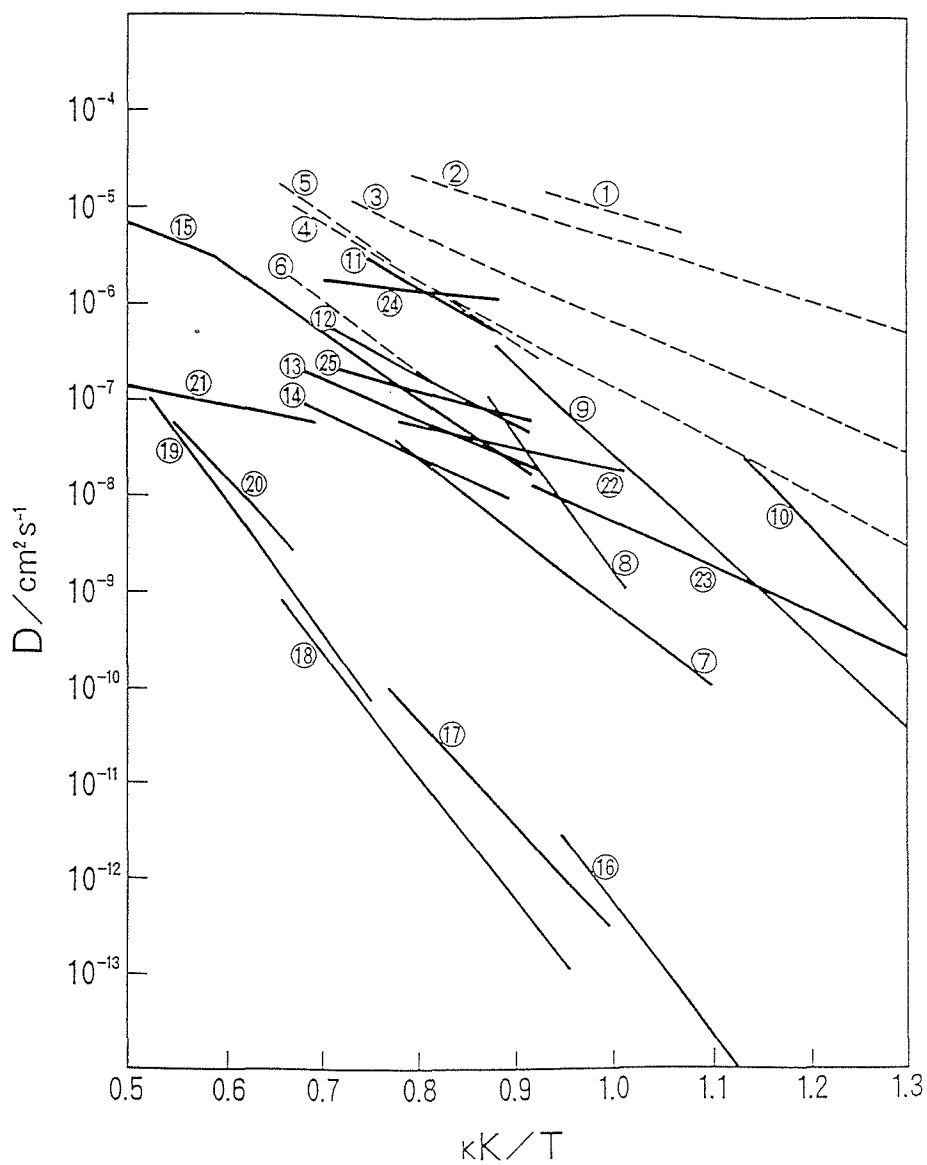
Fig. 27 Diffusion constants of anion sublattice in various fluorite compounds (1).
① δ - Bi_2O_3, ② $Ce_{1.8}$ $Gd_{0.2}$ $O_{1.9}$, ③ $(ZrO_2)_{0.9}$ $(Y_2O_3)_{0.1}$, ④ $(CaO)_{0.13}$
$(ZrO_2)_{0.87}$, ⑤ $(ThO_2)_{0.93}$ $(Y_2O_3)_{0.07}$, ⑥ $(CaO)_{0.12}$ $(HfO_2)_{0.88}$.
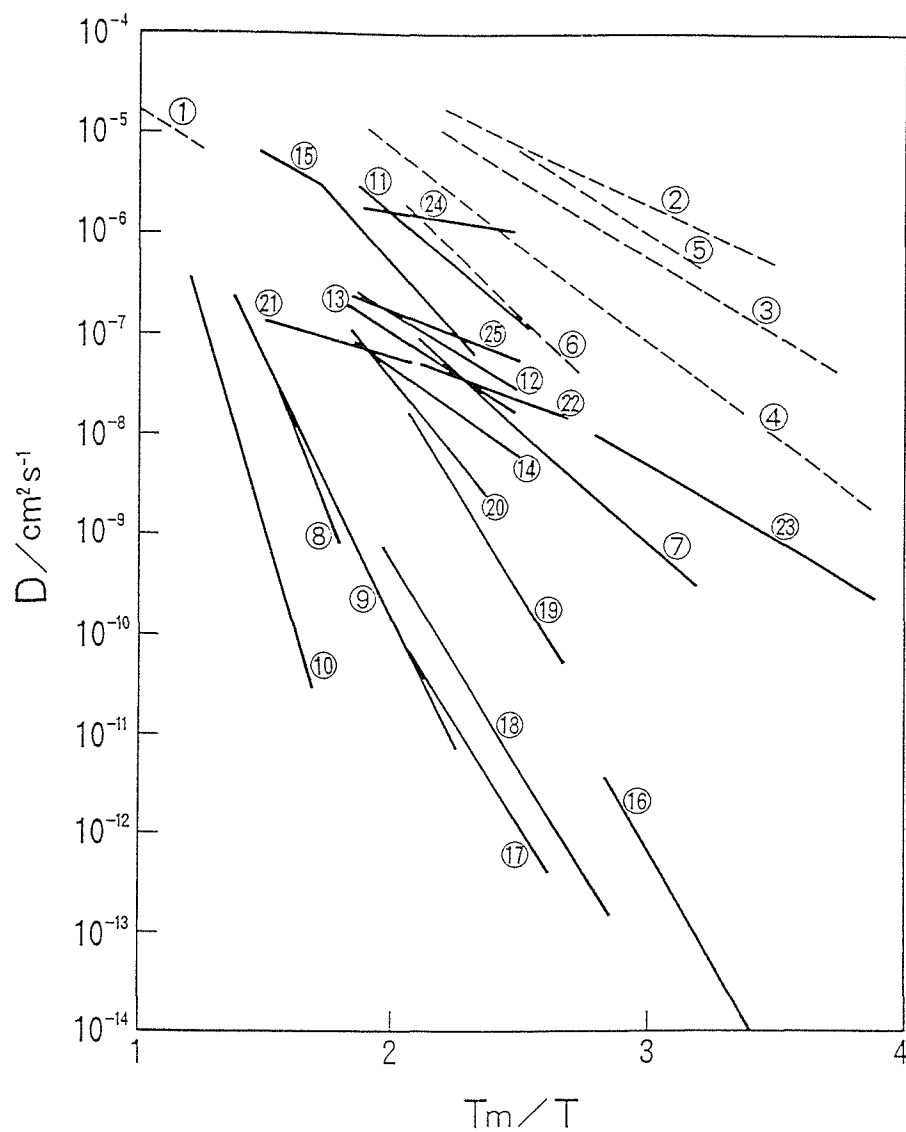The data marked 7 - 25 are the same as those in the caption of Fig. 26.

Fig. 28 The diffusion constants of anion sublattice in various fluorite compounds as a function of normalized temperature. The compounds marked 1 - 25 are the same as those in the caption of Fig. 27.
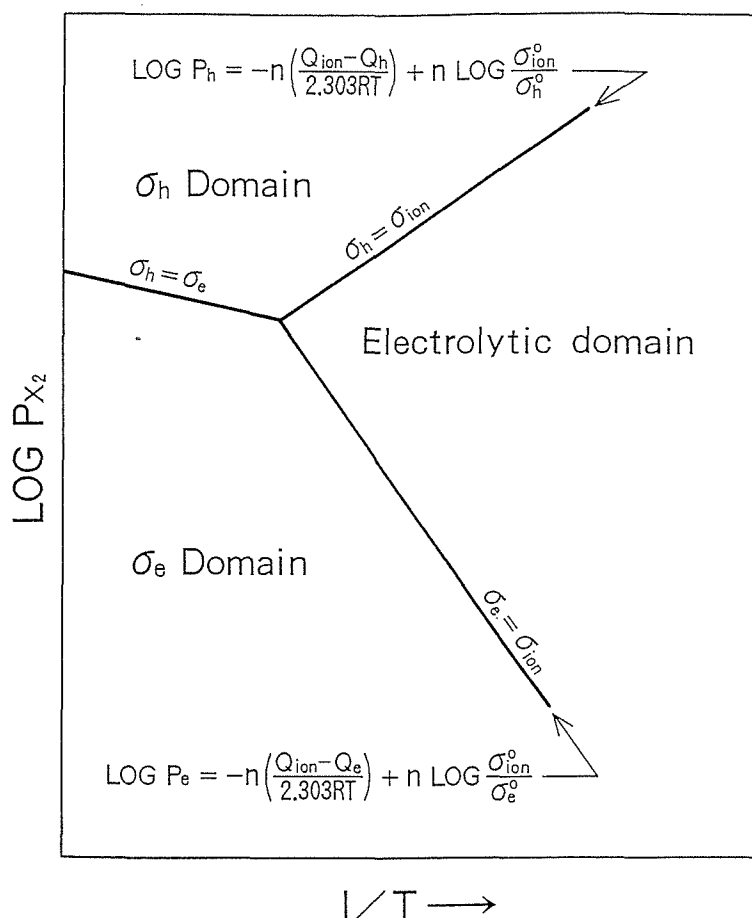
Fig. 29 Relationship between the electrolyte domain and electronic domains in the log P_{x_2} versus $1/T$ plane (41).

according to Eq. (3) and taking $t_i = 0.5$ as functions of temperature and pressure. The results of ionic transference number measurements for yttria - doped ceria measured by Tuller and Nowick (42) are shown in Fig. 30 as an example.

The ionic transference number decreases when the temperature increases and oxygen partial pressure decreases, because doped ceria shows a n - type conduction at low oxygen partial pressures and high temperatures as:

$$O_o = 1/2O_2 + V_o^{\cdot\cdot} + 2e, \qquad (33)$$
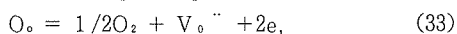
and the number n in Eq. (32) becomes 4 in this case. The electrolyte domains for various fluorite oxides are compiled from the references

(41 - 45) and are shown in Fig. 31, where the inner zones of shaded marks show electrolyte domain. As shown, thoria - and zirconia-based oxides show a wide range of electrolyte domain even at low oxygen pressures. Doped Bi_2O_3 and ceria are less stable at low oxygen pressures. The effect of dopants among ceria - based oxides on the critical oxygen pressure, PO_2^*, at $t_i = 0.5$ and 1073K was studied by Yashiro et al. (9) and the results are shown in Fig. 32, where PO_2^* is plotted against the radius of dopant ion. PO_2^* becomes minimum around 0.11nm of the dopant radius. This figure is analogous to Fig. 9, where the

electrical conductivity shows maximum around 0.11nm of the dopant radius. This relationship suggests that to maximize the electrical conductivity is also effective to maximize the region of electrolyte domain. Since PO_2^* is a measure of reducibility of oxides, the reduction experiment was also conducted by Yashiro et al. (9). The weight loss of sample expressed as the deviation from stoichiometry, δ, in $(CeO_{2-\delta})_{0.8}$ $(LnO_{1.5})_{0.2}$ where Ln = Sm, Gd, Nd and Yb is shown in Fig. 33. As seen in Fig. 33, Sm-doped ceria is most stable against reduction. The attempt to increase the electrolyte domain was conducted on $Ce_{0.8}Gd_{0.2}O_{2-y}$ by Maricle et al. (46) by doubly doping Pr in gadlinia - doped ceria. As shown in Fig. 34, the critical oxygen partial pressure PO_2^* decrease by about two orders of magnitude by doping 3% Pr in gadlinia - doped ceria.
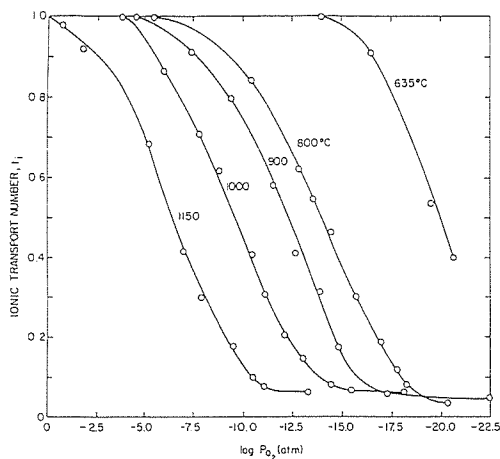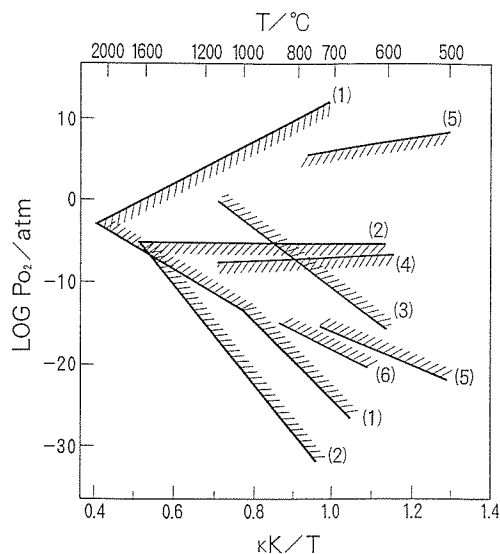

Fig. 31 The electrolyte domains (ti~1) for various fluorite oxides. (1) CSZ (42), (2) YDT (42), (3) $(Y_2O_3)_{0.05}$ $(CeO_2)_{0.95}$ (41), (4) $(CaO)_{0.15}$ $(La_2O_3)_{0.85}$ (43) (5) $(Y_2O_3)_{0.27}$ $(Bi_2O_3)_{0.73}$ (44), (6) $Ce_{0.8}Gd_{0.2}O_{1.9}$ (45).

Fig. 30 The ionic transference number of yttria - doped ceria as a function of PO_2 for various temperatures (42).
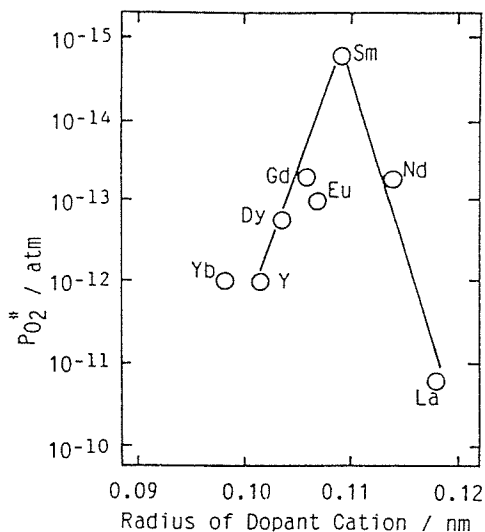

Fig. 32 Correlation between the critical oxygen partial pressure (at $t_i = 0.5$) and the radius of dopant cation of ceria based oxides (9).
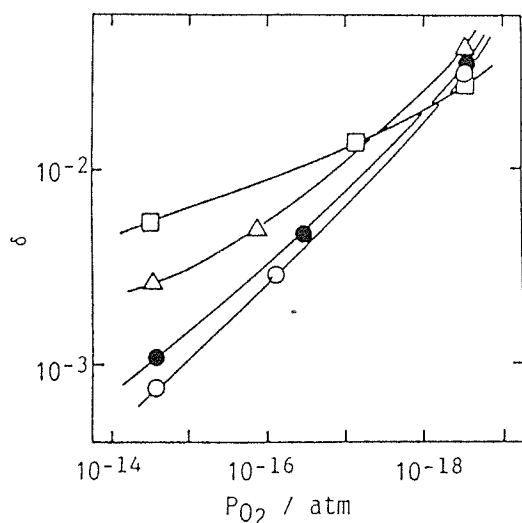
Fig. 33 Isothermal plots of weight loss with the deviation from nonstoichiometry, δ, versus oxygen partial pressure for (Ce $O_{2-\delta})_{0.8}$ (LnO$_{1.5})_{0.2}$ at 1073K (9); $\bigcirc$ Sm, $\bullet$ Gd, $\triangle$ Nd, $\square$ Yb.
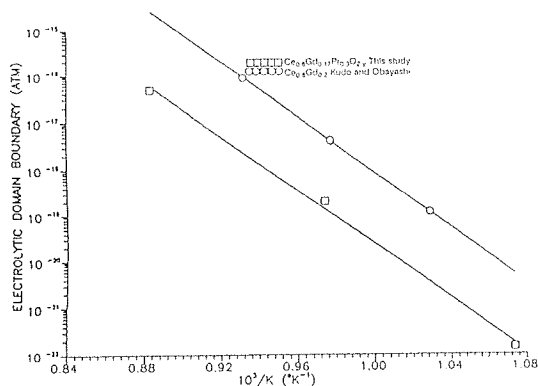

Fig. 34 The effect of double doping of Pr in gad linia - doped oxides on the critical oxygen partial pressure (46).

8. The effect of sample preparation

The electrical conductivities of Ce$_{0.8}$ Gd$_{0.2}$ O$_{1.9}$ obtained from various authors (10, 11, 45, 47) are shown in Fig. 35. This figure would show that the electrical conductivity is dependent on sample preparation: powder of raw materials, impurities, sintering condition and so on.

The both plots of (2) and (3) in Fig. 35 are

obtained by Riess et al. (47) and the former sample was obtained from the coprecipitation method with a narrow distribution of powder size and the latter from the mixing of CeO$_2$ and Gd$_2$O$_3$ with a wide distribution of powder size.
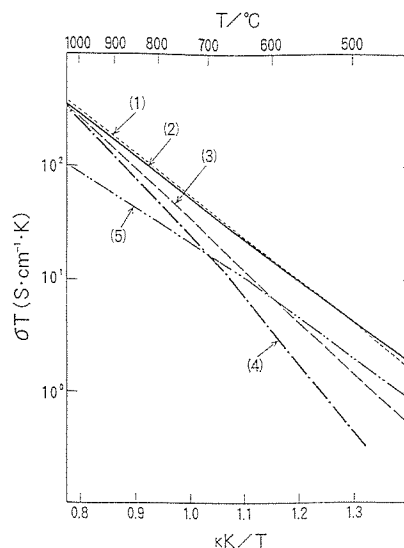

Fig. 35 The variation of electrical conductivity of Ce$_{0.8}$ Gd$_{0.2}$ O$_{1.9}$ obtained from different authors and different methods. (1): (45), (2): (47), (3): (47), (4): (10), (5): (11).

They regarded the difference in the electrical conductivity of gadlinia - doped ceria as imhomogeneity in the Gd distribution and the larger activation energy was interpreted as due to the formation of Gd - rich grain boundary.

The effect of density and impurities was studied by Gerhardt and Nowick (48) and the results are shown in Fig. 36 and 37, respectively. The effect of density is rather small as seen in Fig. 36, but the impurity of Si makes the electrical conductivity of grain boundary larger drastically as seen in Fig. 37. This effect is interpreted as due to the formation of high resistive glassy phase in the grain boundary.
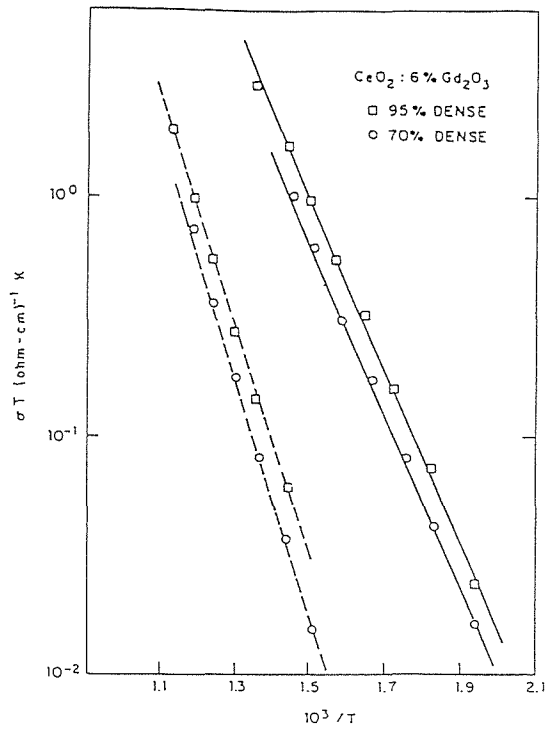
Fig. 36 Electrical conductivity curves of two
samples of gadlinia - doped ceria with
different density. Solid lines represent
the bulk behavior and the broken lines
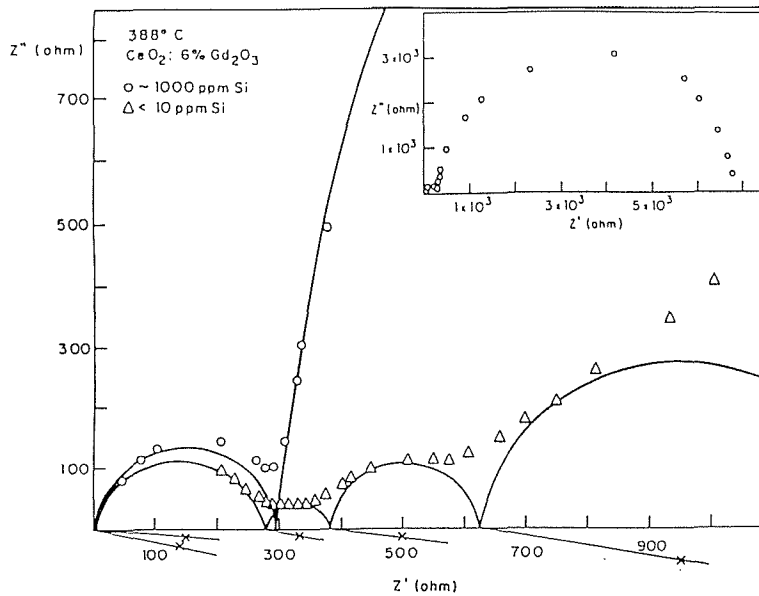the grain - boundary behavior (48).

Fig. 37 Complex impedance curves at 388℃ of two gadlinia - doped ceria prepared with different
starting materials: open circles are for the conventional samples containing 1000ppm Si,
whereas triangles are prepared from "Si - free" (⟨10ppm) material. The inset shows the
complete second arc for the sample containing 1000ppm Si (48).

9. Concluding remarks

The diffusion constants of ceria - based oxides are estimated to be almost the highest among the fluorite oxides by comparing the diffusion data of these oxides using the Nernst - Einstein relationship. The pre - exponential term and the activation energy of the electrical conductivity of ceria doped with tri - valent cation can be expressed as:

$$A = (4e^2/kW)a^2v_0 \, N_0 \exp(\Delta S_m/k)$$
$$\exp(\Delta S_{A1}/k) \qquad (34)$$
$$E_a = \Delta H_m + \Delta H_A \qquad (35)$$

In order to search the oxides with higher electrical conductivity the following points should be considered.

(1) Since ΔS_m is considered to be constant when the host lattice is determined, maximization of v_0 and ΔS_{A1} is necessary in order to increase A in Eq. (28). The increase in v_0 at a given temperature may be achieved by lowering the melting point of the oxides, since the plot of the diffusion constant against the normalized temperature approaches 10^{-4} cm^{2}s^{-1} at the melting point. The mechanism to increase ΔS_{A1} is not clear at present, but it would be effective to doubly or triply dope proper ions in order to suppress the defects ordering.

(2) In order to lower activation energy, the association enthalpy ΔH_{A1} in Eq. (35) should be minimized since ΔH_m is considered to be constant. The theoretical prediction to minimize ΔH_m is rather apparent as was discussed in section 4. The optimum radius of dopant cations should be the critical radius, which is about 0. 111 and 0. 104 nm for di - valent and tri - valent cations in the ceria - based oxides, respectively. In order to obtain the lattice constant with no expansion nor contraction in doubly or triply doped ceria, the combination of dopant cations so as to obtain the same value as average as the critical radius of the one dopant system would be effective.

The increase in the region of electrolyte domain of doped ceria is also an important problem, because it is apt to be reduced and electronic conduction becomes significant at low oxygen partial pressures. In order to increase the electrolyte domain, to increase in the ionic conductivity by any means, of course, is effective. It is suggested that the doubly doping of Pr is effective to increase the electrolyte domain without changing the magnitude of ionic conductivity.

The importance of the method for the sample preparation is also described. The most serious problem in the sample preparation of rare earth - doped ceria would be the homogeneity of rare earth atoms in the sample, since electrical conduction is much dependent on the concentration of rare earth elements. The inclusion of impurity Si drastically increases the grain boundary resistivity by making high resistivity layer including Si in the grain boundary.

10. Acknowledgement

11. References

(1) B. C. H. Steele in "High Conductivity Solid Ionic Conductors," T. Takahashi, ed., World Scientific Publishing Co., Singapore (1989).

(2) J. A. Kilner and B. C. J. Steele in "Nonstoichiometric Oxides," O. T. Sorensen, ed., Academic Press, New York (1981).

(3) K. Sasaki, a doctoral dissertation submitted to the Swiss Federal Institute of Technology, Zurich (1993).

(4) R. M. Dell and A. Hooper, p. 291 in "Solid Electrolytes," P. Hagenmüller and W. Van Gool, ed., Academic Press (1978).

(5) J. A. Kilner and C. D. Walters, Solid State Ionics, **6** (1982) 253.

(6) M. A. Panhans and R. N. Blumenthal, Solid State Ionics, **60** (1993) 279.

226

(7) H. Yashiro, T. Ohuchi, K. Eguchi and H. Arai, J. Mater. Sci. **23** (1988) 1036.

(8) H. Arai, T. Kunisaki, Y. Shimizu, and T. Seiyama, Solid State Ionics **20** (1986) 241.

(9) H. Yashiro, K. Eguchi and H. Arai, Solid State Ionics **36** (1989) 71.

(10) G. B. Balazs and R. S. Glass, p. 478 in the Proceedings of the Second International Symposium on "Ionic and Mixed Conducting Ceramics", T. A. Ramanarayanan, W. L. Worrell and H. L. Tuller, ed., The Electrochemical Society, Inc., (1994).

(11) K. Eguchi, T. Setoguchi, T. Inoue and H. Arai, Solid State Ionics **52** (1992) 165.

(12) R. Gerhardt - Anderson and A. S. Nowick, Solid State Ionics **5** (1981) 547.

(13) R. T. Dirstine, R. N.Blumenthal and T. F. Kuech, J. Electrochem. Soc. **126** (1979) 264.

(14) H. Yashiro, Y. Eguchi, K. Eguchi and H. Arai, J. Appl. Electrochem. **18** (1988) 527.

(15) Da Yu Wang, D. S. Park, J. Griffith and A. S. Nowick, Solid State Ionics **2** (1981) 95.

(16) J. Faber, C. Geoffroy, A. Roux, A. Sylvestre and P. Abelard, Appl. Phys. **A49** (1989) 225.

(17) D. J. M. Bevan and E. Summerville, in : Handbook on the physics and chemistry on rare earth's, Vol. 4, eds., K. A. Gschneider and L. Eyring (North - Holland, Amsterdam, 1979).

(18) V. Bulter, C. R. A. Catlow, B. E. F. Fender and J. H. Harding, Solid State Ionics **8** (1983) 109.

(19) J. A. Kilner, Solid State Ionics **8** (1983) 201.

(20) J. A. Kilner and r. J. Brook, Solid State Ionics **6** (1982) 237.

(21) D. - J. Kim, J. Am. Ceram. Soc. **72** (1989) 1415.

(22) R. D. Shannon and C. T. Prewitt, Acta Cryst. **B25** (1969) 925.

(23) K. Fuda, K. Kishio, S. Yamauchi, K. Fueki and Y. Onoda, J. Phys.Chem. Solids **45** (1984) 1253.

(24) S. B. Adler and J. W. Smith, Chem. Soc. Farad.Trans. **89** (1993) 3123.

(25) J. G. Allpress and H. J. Rossell, J. Solid State Chem. **15**, (1975) 68.

(26) Y. Oishi, K. Ando and M. Akiyama, Bull. Chem. Soc. Jpn. **9** (1981) 1445.

(27) K. Ando and Y. Oishi, J. Nucl. Sci. Technol. **20** (1983) 973.

(28) Hj. Matzke, J. Mater. Sci., **5** (1970) 831.

(29) M. Beniere and C. Chemla, J. Phys. Chem. Solids, **40** (1979) 729.

(30) J. M. Floyd, Ind. J. Technol. **11** (1973) 589.

(31) L. A. Simpson and R. E. Carter, J. Am. Ceram. Soc. **49** (1966) 139.

(32) A. B. Auskern and J. Belle, J. Nucl. Mater., **3** (1961) 267.

(33) R. L. Deaton and C. J. Wiedenheft, J. Inorg. Nucl. Chem., **35** (1973) 649.

(34) J. F. Martin and P. Contamin, J. Nucl. Mater., **30** (1969) 16.

(35) H. S. Edwards, A. F. Rosenberg, and J. T. Bittel, Aeronautical System Division, Wright - patterson Air Force Base, OH, ASD - TDR - 63 - 635, (1963).

(36) K. Ando, Y. Oishi and Y. Hidaka, J. Chem. Phys., **65** (1976) 2751.

(37) K. C. Kim and D. R. Olander, J. Nucl. Mater., **102** (1981) 192.

(38) A. S. Bayoglu and R. Lorenzelli, J. Nucl. Mater., **82** (1979) 403.

(39) P. Contamin, J. J. Bacmann and J. F. Martin, J. Nucl. Mater., **42** (1972) 54.

(40) Hj. Matzke, Proc. 5th Intern. Conf. on Plutonium and Other Actinides 1975 (1976) 801.

(41) J. W. Patterson, J. Electrochem. Soc. **118** (1971) 1033.

(42) H. L. Tuller and A. S. Nowick, J. Electrochem. Soc. **122** (1975) 255.

(43) T. H. Estell and S. N. Flengas, J. Electrochem. Soc. **116** (1969) 771.

(44) T. Takahashi and H. Iwahara and T. Esaka, J. Apple. Electrochem. **7** (1977) 303.

(45) T. Kudo and H. Obayashi, J. Electrochem. Soc. **123** (1976) 415.

(46) D. L. Maricle, T. E. Swarr and S. Karavolis, Solid State Ionics **52** (1992) 173.

(47) I. Riess, D. Braunshtein and D. S. Tannhauser, J. Am. Ceram. Soc. **64** (1981) 479.

(48) R. Gerhardt and A. S. Nowick, J. Am. Ceram. Soc., **69** (1986) 641.